

1 **Acid leaching on the denitrification efficiency of MnCe@FA**
2 **catalyst derived from fly ash: Structure, crystal phase and active**
3 **component interaction**

4 Liguo Chen^{a†}, Mutao Xu^{a,b†}, Yongzhong Wang^c, Qijie Jin^{a*}, Jing Song^d,
5 Changcheng Zhou^d, Jisai Chen^c, Jian Yang^b, Haitao Xu^{a,d*}

6 *a School of Environmental Science and Engineering, Nanjing Tech University,*
7 *Nanjing 210009, PR China*

8 *b College of Materials Science and Engineering, Nanjing Tech University, Nanjing*
9 *210009, PR China*

10 *c Kelin Environmental Protection Technology Co., Suzhou 215200, PR China*

11 *d Nanjing Gekof Institute of Environmental Protection Technology & Equipment Co.,*
12 *Nanjing 210031, PR China*

13 *e CSSC Luzhou Environment Protection (Nanjing) Co., Nanjing 211100, PR China*

14

15 [†]These authors contributed equally to this work.

16 *Corresponding authors: Haitao Xu, Qijie Jin

17 E-mail address: htxu@njtech.edu.cn, qijiejin@njtech.edu.cn

18

19

20

21

22 **Table of contents in Supporting Information:**

23 **Text 1. Experimental section**

24 Tab. S1 Comparison of the efficiency of transition metal and rare earth metal

25 composite denitrification catalysts

26 Tab. S2 Relative element content on the surface of 0.1MC@FA (1) catalyst

27 Fig. S1 Catalyst activity evaluation device diagram

28 Fig. S2 The elemental mappings of 0.1MC@FA(0) catalysts

29 Fig.S3 O₂ adsorption capacity of 0.1MC@FA catalyst

30 Fig. S4 H₂ consumption of 0.1MC@FA catalyst

31 Fig. S5 Denitration efficiency diagram of commercial low temperature denitration

32 catalyst

33 **Text 1. Experimental section**

34 **1. Chemicals and Materials**

35 All chemicals are purchased from the market and used directly without treatment.
36 Copper nitrate trihydrate ($\text{Ce}(\text{NO}_3)_3 \cdot 6\text{H}_2\text{O}$), manganese acetate tetrahydrate
37 $(\text{CH}_3\text{COO})_2\text{Mn} \cdot 4\text{H}_2\text{O}$ and hydroxyethyl cellulose were purchased from Shanghai
38 McLean Biochemical Technology Co., Ltd. The water used is deionized water
39 prepared in the laboratory. The fly ash used in the experiment was taken from
40 Taizhou Power Plant.

41 **2. Material characterization methods**

42 The X-ray diffraction (XRD) patterns were obtained using an X-ray diffractometer
43 (Smartlab TM 3 kW, Rigaku). The scanning speed was $10^\circ \cdot \text{min}^{-1}$, and the 2θ
44 scanning range was $10^\circ - 85^\circ$. The microstructure and element mapping of the
45 catalyst were studied by scanning electron microscopy (JEOL, JSM-5900). X-ray
46 photoelectron spectroscopy (XPS) images were obtained by AXIS ULTRA DLD
47 instrument (Al-K α radiation, 1486.6 eV), and the vacuum was maintained at 10^{-7} Pa.
48 The samples were dried at 100°C . for 24 h to remove water and then tested. The
49 obtained curves were fitted using XPSPEAK 4.1 software. The NH_3 temperature-
50 programmed desorption (NH_3 -TPD) test was performed on CHEMBET-3000
51 (Quantachrome) to obtain the surface acidity of the catalyst. All catalysts were
52 preheated at 400°C . for 1 h under helium flow and then cooled to 50°C . for NH_3
53 adsorption. NH_3 was then desorbed from 50°C to 900°C . at a heating rate of 10
54 $^\circ\text{C} \cdot \text{min}^{-1}$. H_2 temperature programmed reduction (H_2 -TPR) was performed using a

55 semi-automatic Micromeritics TPD/TPR 2900 instrument. All catalysts were
56 preheated at 400 °C for 1 h under argon flow and cooled to 50 °C. Then it was
57 switched to 5 % H₂/Ar and the temperature was increased from 50 °C to 800 °C at a
58 heating rate of 10 °C·min⁻¹. Data are collected over the entire temperature range. TG
59 and DSC data were obtained using a thermogravimetric analyzer (TGA550, America).
60 The heating rate was 10 °C·min⁻¹, the protective atmosphere was air, and the airflow
61 rate was 40 mL·min⁻¹.

62 In situ diffuse reflectance infrared spectroscopy (in situ DRIFTS) was collected by
63 Nicolet is 50 spectrometer. All catalysts were preheated at 400 °C for 2 h under
64 nitrogen flow, and then cooled to the desired temperature. For NH₃ adsorption and
65 NO + O₂ adsorption, when the temperature is cooled to 200 °C, 1000 ppm NH₃ or
66 1000 ppm NO + 10 vol. % O₂ is pumped into the system for 30 min. Then the in situ
67 DRIFT spectra were collected with increasing temperature. For the reaction of NH₃
68 and pre-adsorbed NO + O₂, 1000 ppm NO + 10 vol. % O₂ was pumped into the
69 system for 30 min. After the temperature rises to 400 °C., the flow of NO + O₂ is
70 stopped and N₂ is pumped into the system for 30 min. Then, 1000 ppm NH₃ was
71 pumped into the system and in situ DRIFT spectra were collected with increasing
72 temperature. For the reaction between NO + O₂ and pre-adsorbed NH₃, the gas order
73 is opposite, but the steps are similar to the reaction between NH₃ and pre-adsorbed
74 NO + O₂.

75 **3 Catalyst activity test**

76 The catalyst (1 ml) was added to a fixed-bed quartz reactor (inner diameter 8 mm,

as shown in Fig. S1) to study the NH₃-SCR catalytic activity. The gas flow rate of 500 ml·min⁻¹ corresponds to the volume space velocity (GHSV) of 30000 h⁻¹. The reaction gas is composed of 500 ppm NO, 500 ppm NH₃ (when used), 6 vol. % O₂, and the remaining gas is N₂. The NO concentration at the inlet and outlet of the reactor was obtained by a flue gas analyzer (MRU VarioPlus, Germany). The catalytic activity was calculated by Eq. (1).

$$NO \text{ conversion} = \frac{[NO]_{in} - [NO]_{out}}{[NO]_{in}} \times 100\% \quad \text{Eq. (1)}$$

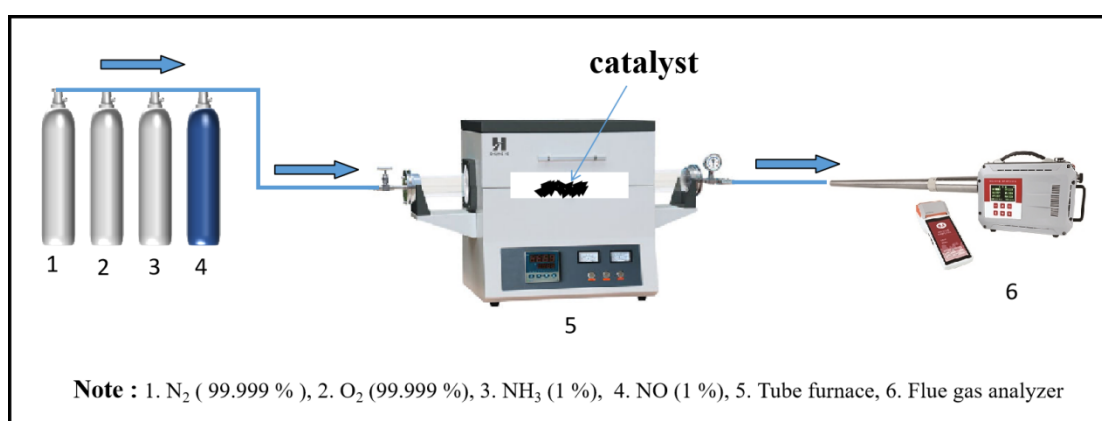


Fig.S1 Catalyst activity evaluation device diagram

Tab. S1 Comparison of the efficiency of transition metal and rare earth metal composite denitrification catalysts

Catalyst	NO _x conversion	Temperature	Ref.
4FeMn ₇ Ce ₃	98%	150 °C	1
Mn-Ce/FA	89.4%	250 °C	2
MnMoVO _x	100%	250 °C	3
NbFeMnCeO _x	91%	200 °C	4
Nb _{0.05} Ce _{0.05} MnO _x	>91%	125-250 °C	5
0.1MnCe@FA	87%	250 °C	This work

Tab. S2 Relative element content on the surface of 0.1MC@FA (1)catalyst

Element	wt. %	σ
Ce	42.3	0.6
Mn	28.6	0.5
O	27.9	0.6
Si	0.8	0.1
Al	0.5	0.1
Ti	0.0	0.0

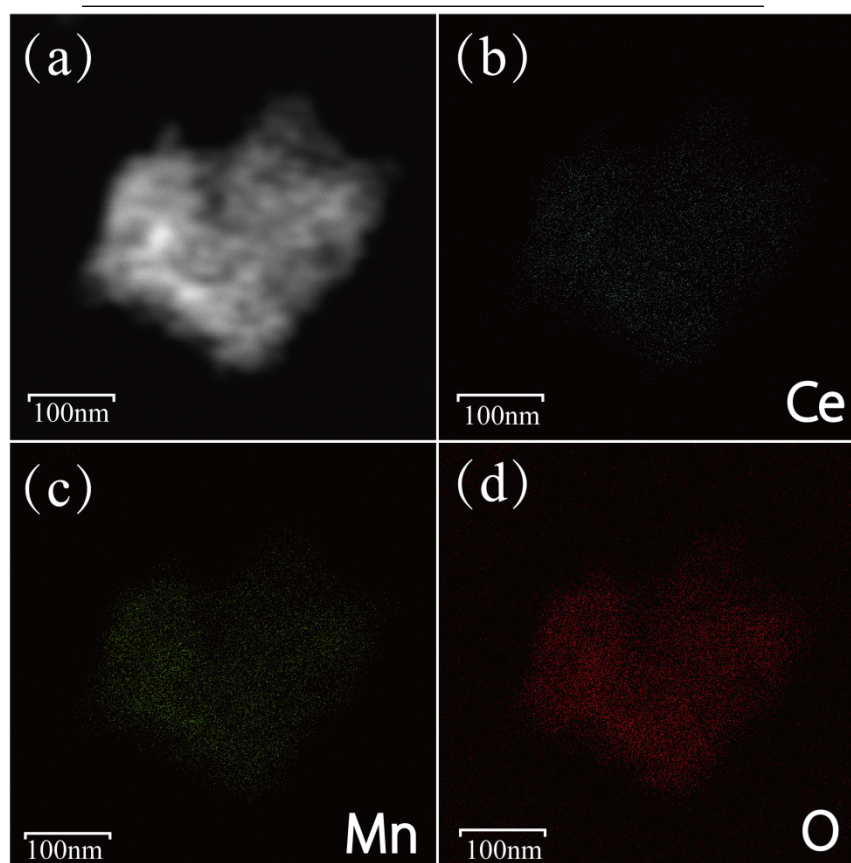


Fig. S2 The elemental mappings of 0.1MC@FA(0) catalysts

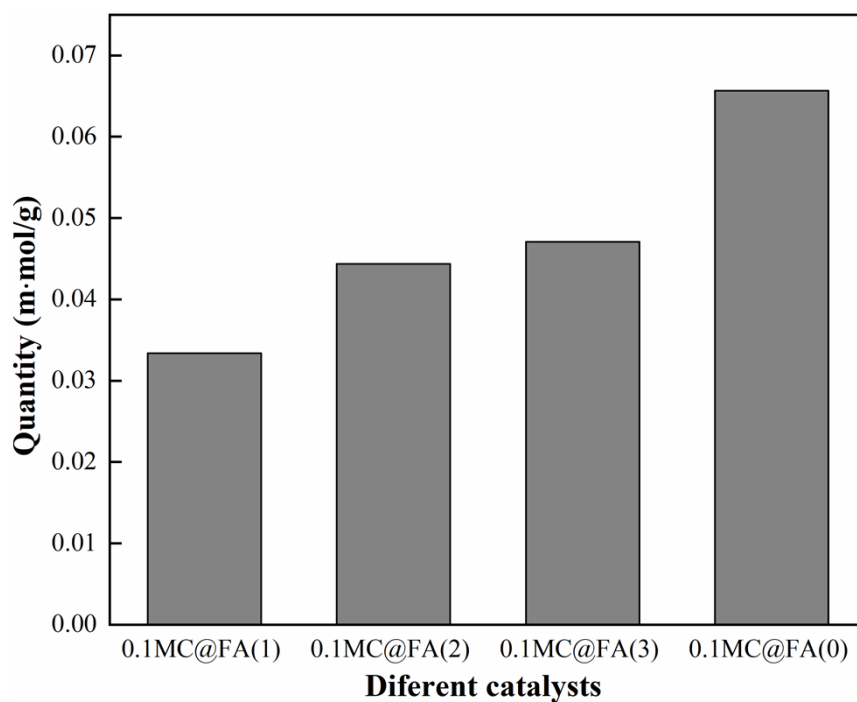


Fig.S3 O₂ adsorption capacity of 0.1MC@FA catalyst

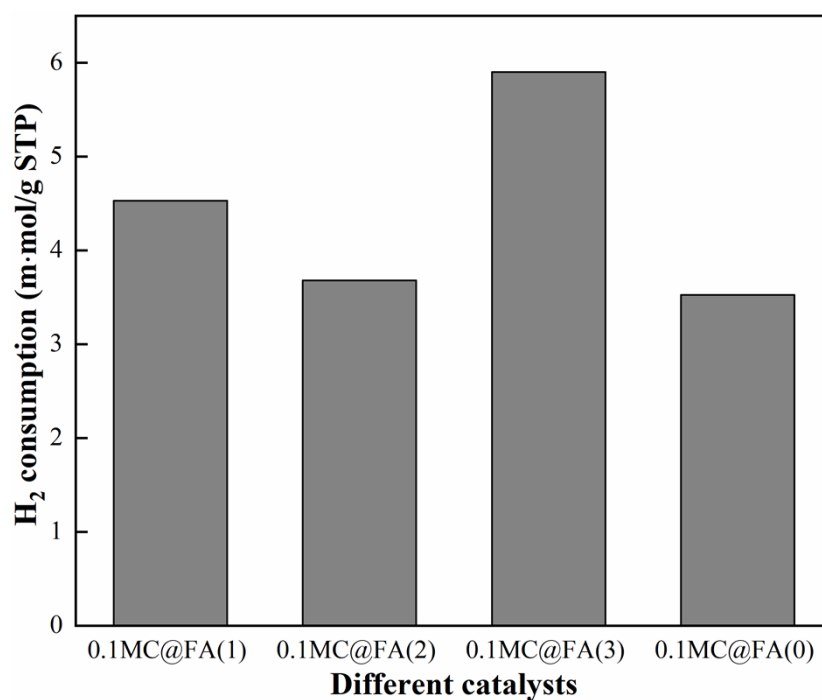


Fig. S4 H₂ consumption of 0.1MC@FA catalyst

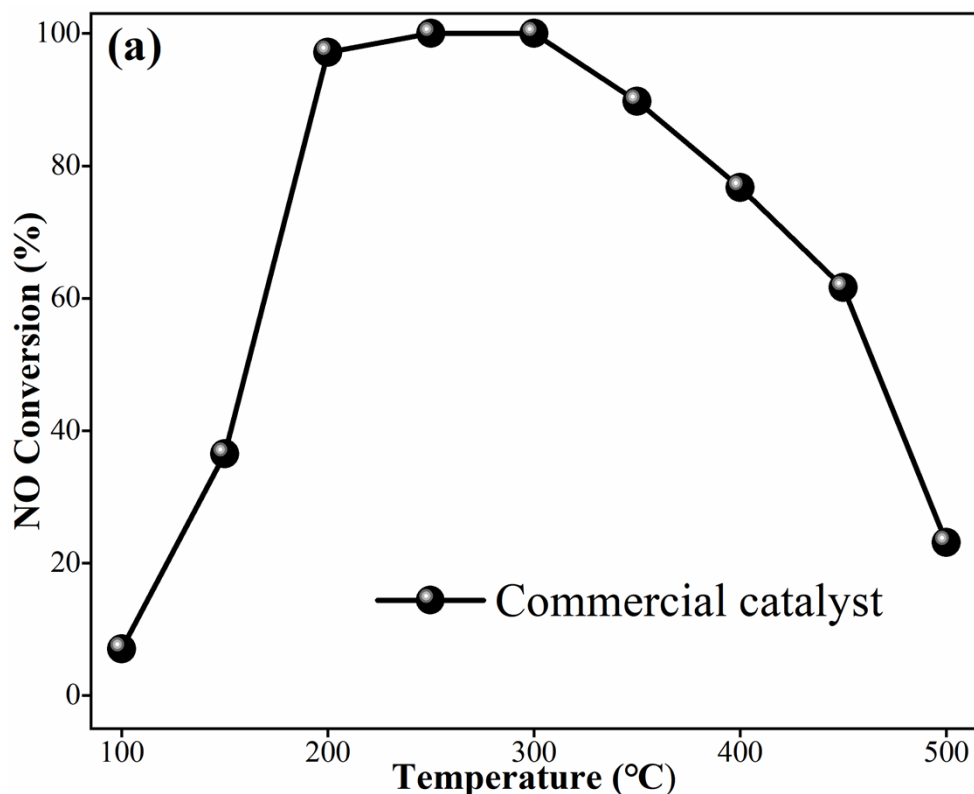


Fig. S5 Denitration efficiency diagram of commercial low temperature denitration catalyst

Reference

1. S. L. Zhao, J. L. Peng, Y. X. Qian, et al., Low-temperature DeNO_x characteristics and mechanism of the Fe-doped modified CeMn selective catalytic reduction catalyst, *Fuel Process. Technol.*, 2023, **244**, 107704.
2. P. Zhang, W. H. Yu, B. Gao, et al., Denitration performance and mechanism of Mn-Ce supported alkali-modified fly ash catalysts for NH₃-SCR, *Fuel*, 2023, **357**, 129878.
3. Y. L. Li, G. B. Li, Y. Zou, et al., Unveiling the remarkable deNO_x performance of MnMoVO_x catalysts via dual regulation of the redox and acid sites, *Applied Catalysis B: Environment and Energy*, 2023, **344**, 123612.
4. L. L. Long, S. H. Tian, Y. C. Zhao, et al., Promotional effects of Nb⁵⁺ and Fe³⁺ co-doping on catalytic performance and SO₂ resistance of MnO_x-CeO₂ low-temperature denitration catalyst, *J. Colloid Interface Sci.*, 2023, **645**, 876-888.
5. Y. P. Yang, S. C. Li, S. L. Shi, et al., Enhancing the K-resistance of MnO_x catalysts via Ce and Nb co-doping for low-temperature NO_x elimination, *Sep. Purif. Technol.*, 2025, **362**, 131768.